THE JOURNAL OF PHYSICAL CHEMISTRY Letters

Letter

Cite This: J. Phys. Chem. Lett. 2019, 10, 3914−3921

pubs.acs.org/JPCL

Ultraviolet to Long-Wave Infrared Photodetectors Based on a Three-Dimensional Dirac Semimetal/Organic Thin Film Heterojunction

Ming Yang,[†] Jun Wang,[*,†,‡] Yunkun Yang,[§] Qi Zhang,[∥] Chunhui Ji,[†] Guorong Wu,[∥] Yuanjie Su,[†] Jun Gou,[†] Zhiming Wu,[†,‡] Kaijun Yuan,[∥] Faxian Xiu,[*,§,⊥] and Yadong Jiang[†,‡]

[†]School of Optoelectronic Science and Engineering, University of Electronic Science and Technology of China, Chengdu 610054, P. R. China

[‡]State Key Laboratory of Electronic Thin Films and Integrated Devices, University of Electronic Science and Technology of China, Chengdu 610054, P. R. China

[§]State Key Laboratory of Surface Physics and Department of Physics, Fudan University, Shanghai 200433, P. R. China

[∥]State Key Laboratory of Molecular Reaction Dynamics, Dalian Institute of Chemical Physics, Chinese Academy of Sciences, Dalian 116023, P. R. China

[⊥]Collaborative Innovation Center of Advanced Microstructures, Nanjing 210093, China

Supporting Information

ABSTRACT: In this work, high-performance ultraviolet to long-wave infrared (UV−LIR) devices based on an N-type three-dimensional (3D) Dirac semimetal Cd_3As_2 and P-type organic (small molecules and polymers) heterojunction are prepared. Primarily, the photodetector shows a broadband photoresponse from 365 to 10600 nm. The optimized device responsivity is 729 mA/W, along with a fast response time of 282 μs and a high on−off ratio of 6268, which are 2 orders of magnitude higher than those previously reported for a 3D Dirac semimetal-based device. In the LIR region (10600 nm), the responsivity and on−off ratio can reach 81.3 mA/W and 100, respectively. In addition, the time-resolved femtosecond pump detection technology is used to reveal the relaxation time of Cd_3As_2/organic thin films (4.30 ps), indicating that Cd_3As_2/organic thin films have great potential for the manufacture of fast IR devices. These results demonstrate that the 3D Dirac semimetal/organic thin film heterojunction photodetectors will be a feasible solution for high-speed and broadband photodetectors in large-array imaging.

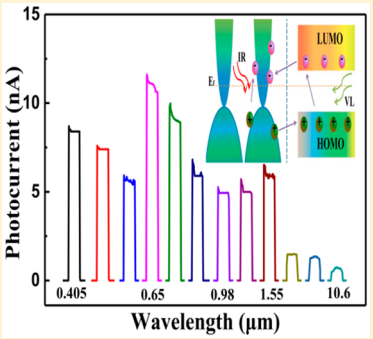

The photodetector is the core of a photoelectric system, which is always research hot spot.[1−4] To overcome the detection waveband limitations of traditional photodetectors, novel infrared (IR) photodetectors based on Dirac materials have gradually emerged due to their zero bandgap and wide spectral absorption.[5−7] As the most outstanding representative of two-dimensional (2D) Dirac materials, graphene has been widely studied due to its excellent carrier transport performance, unique 2D energy dispersion, and stable electrical and optical properties.[8−10] However, the application of graphene is hindered by its monatomic layer as well as the limited absorption (2.3%) and fragile surface boundaries. Hence, three-dimensional (3D) Dirac semimetal materials solve this conundrum.[11−13] Interestingly, this type of material not only possesses the characteristics of zero bandgap and wide spectral absorption like 2D Dirac materials but also has a higher electron mobility and absorbs more light. In addition, it exhibits stable physical and chemical properties and interface characteristics. These characteristics open up various prospects of application for 3D Dirac materials.[14−17]

As a typical 3D Dirac semimetal material, Cd_3As_2 possess an ultrahigh carrier mobility (~10^5), a high level of full spectral absorption (30−50%), a 3D quantum Hall effect, a fast electron transmission speed, and a high photocurrent response, which enable wide applications in IR photoelectric detection.[18−20] Wang et al. prepared devices by using pure Cd_3As_2 nanoplates and nanowires, which had a maximum responsivity (R_i) of 5.9 mA/W and broadband detection capability (from 532 nm to 10.6 μm).[21] In addition, Yavarishad et al. revealed that a room-temperature Cd_3As_2 platelet photodetector exhibited optical spectral response characteristics but the maximum R_i of this device was 0.27 mA/W at 635 nm.[22] In addition, Zhu et al. demonstrated the saturated absorption characteristics of a Cd_3As_2 thin film at wavelengths of 1−2 μm.[23] These studies suggest that Cd_3As_2 possesses excellent optical absorption and photoelectric conversion characteristics and thus is the appropriate material for preparing photoelectric devices. However, pure Cd_3As_2, especially pure thin films, due to their semimetal properties as well as the low surface resistance, results in a large overall dark current of devices and

Received: June 5, 2019
Accepted: June 28, 2019
Published: June 28, 2019

DOI: 10.1021/acs.jpclett.9b01619
J. Phys. Chem. Lett. 2019, 10, 3914−3921

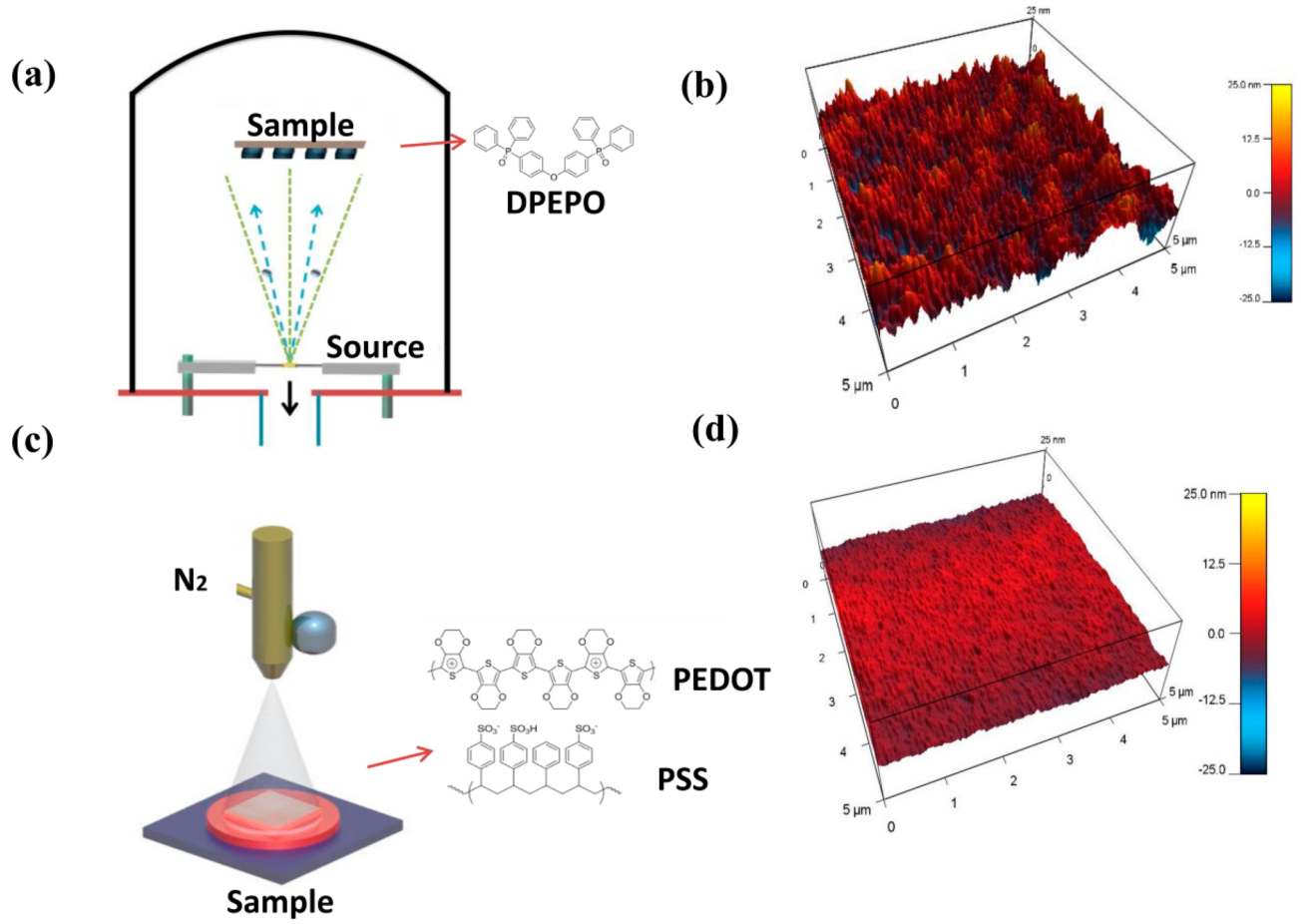

Figure 1. Molecular structure of different organic materials, schematic diagram of the equipment used to prepare thin films, and AFM diagram of different organic thin films on Cd_3As_2 thin films. (a and c) Schematic diagrams of the chemical molecular structure and fabrication equipment (thermal evaporation and spraying) of bis[2-(diphenylphosphino)phenyl] ether oxide (DPEPO) and poly(3,4-ethylenedioxy thiophene):poly-(styrenesulfonate) (PEDOT:PSS), respectively. (b and d) AFM surface diagrams of DPEPO and PEDOT:PSS thin films on a Cd_3As_2 thin film, respectively. The area is 5 μm × 5 μm. Hence, the root-mean-square roughness values of DPEPO and PEDOT:PSS are 7.207 and 3.583 nm, respectively.

has an adverse effect on device sensitivity. To overcome this problem, Yang et al. fabricated a photodetector made of a Cd_3As_2 thin film with pentacene, whose detection range was from 450 nm to 10.6 μm with a maximum R_i of 36.15 mA/W.[24] Nevertheless, the response time of the device is only 60−90 ms, and the switching ratio is 107, which still needs to be improved.

In this paper, Cd_3As_2/organic (small molecules and polymers) heterojunction photodetectors were prepared. More definitively, we combined P-type materials DPEPO (small molecule) and PEDOT:PSS (polymers) with N-type Cd_3As_2 thin films. Such photodetectors can operate under both zero-bias mode and biased mode. Primarily, a Cd_3As_2/small molecule heterojunction photodetector shows an ultrawide response waveband from the ultraviolet (UV) (365 nm) to the long-wave infrared (LIR) (10600 nm). Its R_i can reach 729 mA/W, and its on−off ratio can reach 6286. Then, the problem of forming the polymers on the surface of Cd_3As_2 thin films was solved creatively by a spraying method. Surprisingly, a Cd_3As_2/polymer heterojunction photodetector possesses super fast response times of 282 μs (rise time) and 517 μs (fall time). All of this information fully demonstrates that the combination of Cd_3As_2 thin films with organics has great potential in fabricating high-performance photoelectric devices.

First, a planar structure is adopted to improve the device performance to create the heterojunction. A schematic diagram of the preparation of Cd_3As_2/organic thin film heterojunction photodetectors is shown in Figure S1. For the thin film-type photodetectors, the quality of the prepared thin films will affect the performance of the devices.[25,26] Figure 1 shows the schematic diagram of the equipment used to prepare different thin films and the atomic force microscopy (AFM) surface topography of the surface of the organic thin films (Cd_3As_2 is shown in Figure S2). From Figure 1, one can clearly see that the thin films made of two materials are uniform and compact. Overall, the thin film quality of the two kinds of combined thin films is excellent, which can satisfy the needs of preparing devices (thin film device shown in Figure S3).

Next, we carry out a comprehensive study of the performance of two types of photodetectors (Cd_3As_2/DPEPO and Cd_3As_2/PEDOT:PSS) with respect to the $I-V$ curve of switching illumination, the photocurrent in different wavebands, the effects of V_{bias} on the photocurrent, the on−off ratio, R_i, and EQE (Figure 2).

Panels a and d of Figure 2 show the $I-V$ curve of Cd_3As_2/organic thin films heterojunction devices, in which the Cd_3As_2/polymer thin film heterojunction devices have better rectification characteristics. From the photocurrent diagram

DOI: 10.1021/acs.jpclett.9b01619
J. Phys. Chem. Lett. 2019, 10, 3914−3921

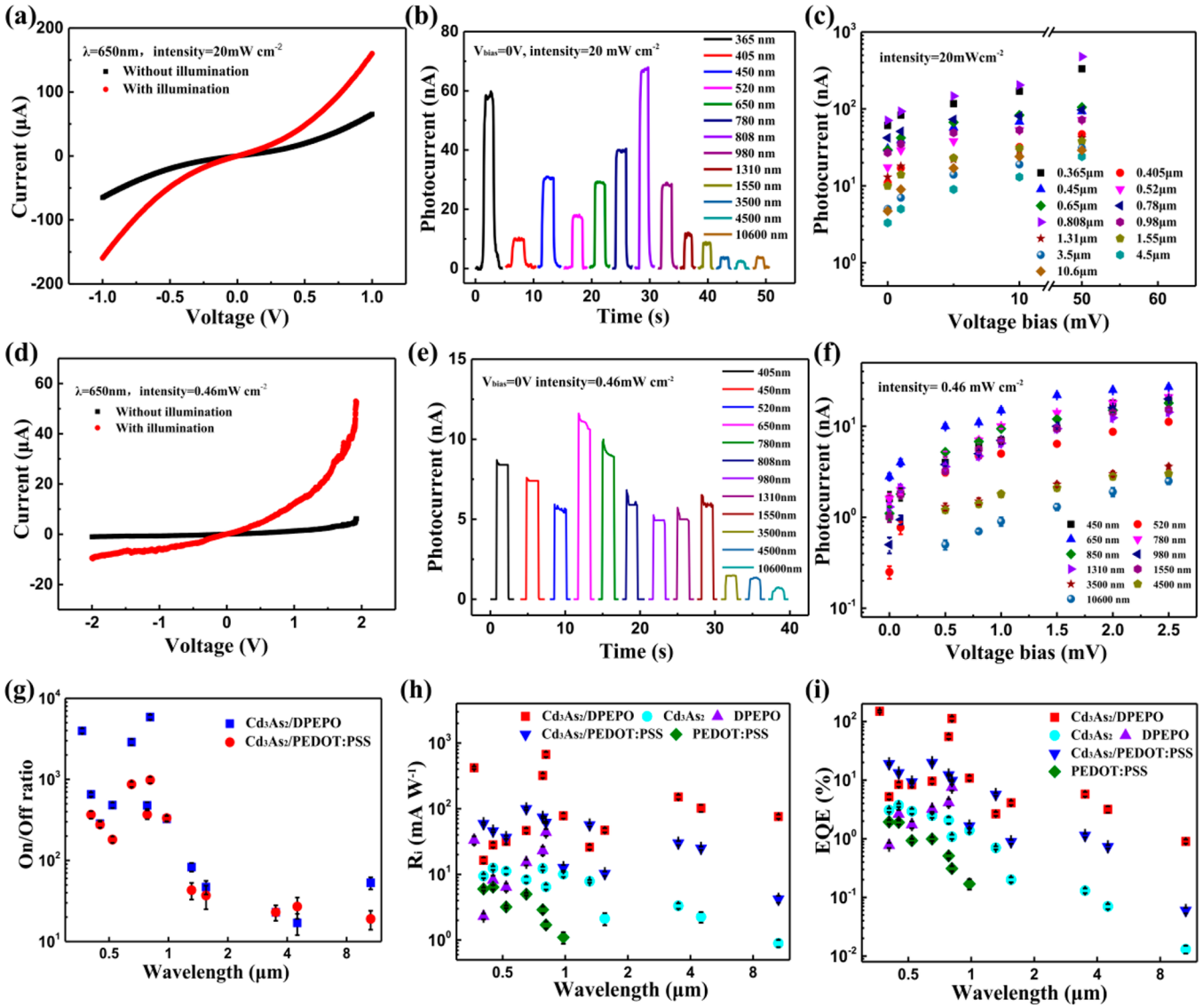

Figure 2. Optoelectronic peculiarity of the Cd_3As_2/DPEPO and Cd_3As_2/PEDOT:PSS heterojunction photodetectors. (a and d) *I*−*V* curves of Cd_3As_2/DPEPO and Cd_3As_2/PEDOT:PSS heterostructure zero-bias photodetectors, respectively, without and with 650 nm irradiation. (b and e) Photocurrents of different wavelengths for Cd_3As_2/DPEPO and Cd_3As_2/PEDOT:PSS heterostructure zero-bias photodetectors, respectively. The measurements were conducted under zero-bias mode with laser power intensities of 20 and 0.46 m/W^2, respectively. (c and f) Photocurrents as a function of different bias voltages for Cd_3As_2/DPEPO and Cd_3As_2/PEDOT:PSS heterojunction photodetectors, respectively. The curve of the variation of the photocurrent with V_{bias} at diverse wavebands. (g) On−off ratios of Cd_3As_2/DPEPO and Cd_3As_2/PEDOT:PSS heterojunction photodetectors at diverse wavelengths. (h and i) R_i and EQE curves, respectively, at different wavelengths of Cd_3As_2/DPEPO, Cd_3As_2/PEDOT:PSS, Cd_3As_2, DPEPO, and PEDOT:PSS photodetectors.

of the zero-bias mode in the different wavebands (Figure 2b,e), one can see clearly that photodetectors possess an excellent response photocurrent from the UV to the LIR. In addition, the photodetectors can produce a much stronger photocurrent when it works under the V_{bias} mode (Figure 2c,f). It is noteworthy that the crest on−off ratio values of Cd_3As_2/DPEPO and Cd_3As_2/PEDOT:PSS photodetectors can reach 6268 (at 650 nm) and 1356 (at 650 nm), respectively. Moreover, what deserves our attention is the fact that the on−off ratio of devices can also reach 22 and 35, 100, and 54 in the MIR (at 4.5 μm) and LIR (at 10.6 μm) regions, which is quite rare for the MIR and LIR photodetectors.

R_i and EQE are calculated to better characterize the excellent performance of the device. R_i is generally defined as the photocurrent generated by the power density of illumination on the active area of the device.

$$R_i = \frac{I_{ph}}{p} = \frac{I_L - I_D}{p} \quad (1)$$

where I_{ph}, I_L, I_D, and p represent the photocurrent generated on the active area, the current under the light, the dark current, and the power density of the laser, respectively.[27−30]

The energy conversion efficiency of illumination is denoted EQE:

$$EQE = \frac{I_{ph}}{q\emptyset} = \frac{h\nu}{q}\frac{I_{ph}}{p} = R_i\frac{h\nu}{q} \quad (2)$$

DOI: 10.1021/acs.jpclett.9b01619
J. Phys. Chem. Lett. 2019, 10, 3914−3921

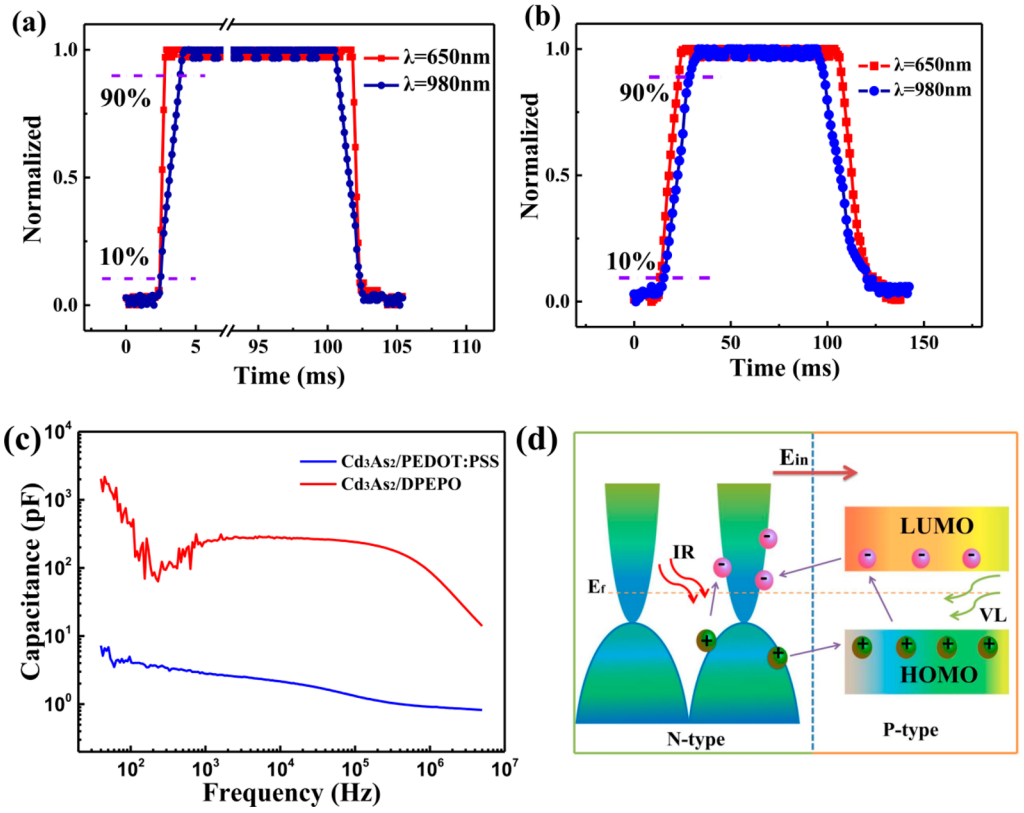

Figure 3. Response time diagram of heterojunction photodetectors at different wavelengths and energy band diagram of the heterojunction. (a and b) Response times of Cd_3As_2/PEDOT:PSS and Cd_3As_2/DPEPO thin film heterojunction photodetectors at 650 and 980 nm. The τ_{on} and τ_{off} of Cd_3As_2/PEDOT:PSS thin film heterojunction photodetectors are 282 and 517 μs and 1.87 and 1.94 ms at 650 and 980 nm, respectively. The τ_{on} and τ_{off} of Cd_3As_2/DPEPO thin film heterojunction photodetectors are 9.7 and 11.49 ms and 16.32 and 23.75 ms at 650 and 980 nm, respectively. (c) The Cd_3As_2/organic thin films capacitance varies with frequency (from 40 to 5.5 × 10^6 Hz). (d) Energy band diagram of Cd_3As_2/organic thin film heterojunction photodetectors. The E_f of Cd_3As_2 is nearly −4.5 eV.[44] The LUMO and HOMO of DPEPO (PEDOT:PSS) are −1 eV (−3.5 eV) and −6.4 eV (−5.2 eV), respectively.

where Ø, q, and $h\nu$ represent the photon flux, the charge per electron, and the photon energy, respectively.[31−33]

The curves of R_i (Figure 2h) and EQE (Figure 2i) of Cd_3As_2/DPEPO, Cd_3As_2/PEDOT:PSS, Cd_3As_2, DPEPO, and PEDOT:PSS photodetectors follow the corresponding formulas mentioned above. The R_i of the photodetectors in this experiment can be as high as 729 mA/W (at 808 nm, Cd_3As_2/DPEPO), which is the maximum for Cd_3As_2-based photodetectors determined to date. The value of R_i is 78 or 186 times that of the pure Cd_3As_2 thin film or the pure Cd_3As_2 crystal devices, respectively. This result is a significant improvement in the performance of Cd_3As_2-based photodetectors. The maximum EQEs of Cd_3As_2/DPEPO and Cd_3As_2/PEDOT:PSS can reach 112% (at 365 nm) and 20.6% (at 650 nm), respectively. In short, Cd_3As_2/DPEPO and Cd_3As_2/PEDOT:PSS thin film heterojunction photodetectors have values of R_i and EQE that are higher than those of the previously described Cd_3As_2-based devices. In general, a Cd_3As_2 thin film is considered as a semimetal; when it combines with organics, the interface between two materials is a Schottky contact. Then, when plentiful electron traps exist in organics, under the action of voltage, these trapped electrons will be transferred to the interface area between the organics and the electrode, which narrows the barrier junction and increases the photocurrent. This tunneling effect is definitely an element that makes the EQE of the inorganic/organic heterojunction devices surpass 100%.

To further characterize Cd_3As_2/organic heterojunction devices, the absorption of Cd_3As_2/organic thin films is precisely measured. Test methods and results are shown in Figure S4, which directly shows that the recombination of Cd_3As_2 with organic thin films can enhance the absorption from the VL to the LIR. Figure S5 illustrates the absorption of organics from the UV to the NIR. One can see that organics have absorption in the measured waveband, and the absorption effect will be enhanced under the combined action of two thin films. This phenomenon can lead to the R_i of Cd_3As_2/organic heterojunction thin film photodetectors being higher than that of pure Cd_3As_2-based devices (Figure 2h).

Moreover, the response time has always been considered to be a significant feature of photoelectric devices.[34−37] Panels a and b of Figure 3 show the response time curves of Cd_3As_2/PEDOT:PSS and Cd_3As_2/DPEPO heterojunction photodetectors at 650 and 980 nm, respectively. Specifically, the τ_{on} and τ_{off} of Cd_3As_2/PEDOT:PSS heterojunction photodetectors are 282 and 517 μs (at 650 nm) and 1.87 and 1.94 ms (at 980 nm), respectively. The τ_{on} and τ_{off} of Cd_3As_2/DPEPO photodetectors are 9.7 and 11.49 ms (at 650 nm) and 16.32 and 23.75 ms (at 980 nm), respectively. In the electron branch, the measurement response time of devices in this experiment can reach 282 μs (τ_{on} of the Cd_3As_2/PEDOT:PSS heterojunction photodetectors), which is the fastest Cd_3As_2-based device to the best of our knowledge. In addition, special attention must be paid to the fact that the interface

DOI: 10.1021/acs.jpclett.9b01619
J. Phys. Chem. Lett. 2019, 10, 3914−3921

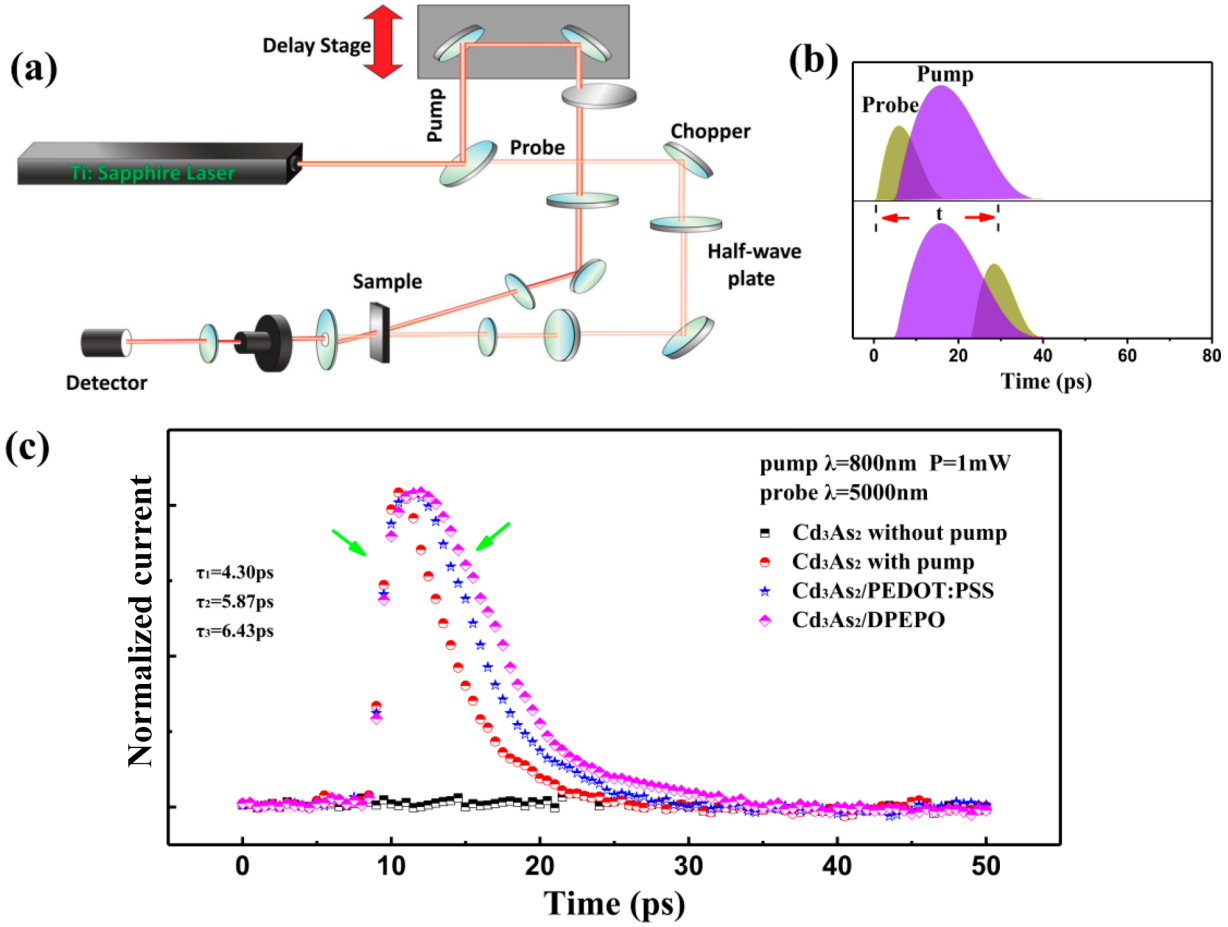

Figure 4. Time-resolved photocurrent measurements of Cd_3As_2/PEDOT:PSS and Cd_3As_2/DPEPO thin films. (a) Schematic diagram of the time-resolved femtosecond pump detection device. Under the condition of taking the regenerating amplification output of femtosecond laser as the experimental light source (repetition frequency of 1 kHz, wavelength of 800 nm, and pulse width of 100 fs), the incident light is divided into two beams of strong and weak light by the 9:1 spectroscope (Throlabs BSWl 1), the strong reflected light is the pump light, and the weak transmitted light is taken as the detection light. (b) Schematic diagram of a pump−probe photoelectric relaxation time measurement system. (c) Induced photocurrent of the probe with the pump on and off as a function of pump−probe pulse delay. The powers of pump and probe excitation both are 1 mW with a spot diameter of 20 μm. The time constants of different composite thin films are 5.87 ps (Cd_3As_2/PEDOT:PSS) and 6.43 ps (Cd_3As_2/DPEPO) with the function mentioned in the Experimental Section.

characteristics of a Cd_3As_2/DPEPO combined thin film are inferior to those of a Cd_3As_2/PEDOT:PSS thin film (Figure 1), which can affect the performance of devices, especially for the response time characteristics. In panels a and b of Figure 3, the response times of photodetectors at 980 nm are lower than at 650 nm. In general, the response times of photodetectors are included in the photoelectric and thermoelectric response. According to the Seebeck effect, the thermoelectric field will have a stronger inhibitory effect on the thermal diffusion of carriers.[38,39] The IR region of light heating effect is stronger than that of the VL region so that the IR region light reaches the carrier balance time faster than that of the VL region.

It is generally believed that the response times of photoelectric devices are primarily affected by three aspects: (1) diffusion time (τ_p), the time required for photon-generated carriers generated outside the P−N junction region to diffuse into the junction region, (2) drift time (τ_{dr}), the time it takes for photogenic carriers to cross the junction region generated in the p−n junction area, and (3) RC delay time (τ_{RC}), which consists of the p−n junction capacitance and load resistance.[40−43] For semiconductor devices, the response time is mainly affected by the third aspect. The capacitance of a Cd_3As_2/organic thin film changes with frequency as observed in Figure 4c. Cd_3As_2/PEDOT:PSS (Cd_3As_2/DPEPO) thin film capacitance C_p (C_D) and resistance R_p (R_D) are 2.7 pF (242 pF) and 1.2 × 10^7 Ω (6.1 × 10^6 Ω), respectively, at 1 kHz. According to the calculation formula $\tau_{RC} = 2\pi RC$, the response time of the Cd_3As_2/PEDOT:PSS (Cd_3As_2/DPEPO) heterojunction photodetector theoretically is 203 μs (9.12 ms). The organics also contribute to extending the response spectrum (Figure S4), because the carrier mobility of an organic semiconductor should be much lower than that of Cd_3As_2, and the response time in this model should be influenced by not only the RC delay time but also the diffusion time of the photogenerated hole/electron in the organic layer. In that case, the carrier mobility of the composite thin film was tested to calculate the overall diffusion time of the device. The carrier diffusion time of the Cd_3As_2/PEDOT:PSS (Cd_3As_2/DPEPO) composite thin film was calculated, which was 32.6 μs (0.27 ms) (diffusion time calculation method shown in Figure S6). When the diffusion time and RC delay time are combined, the theoretical response time of the device is 235.6 μs (9.39 ms), which is consistent with the actual test values.

DOI: 10.1021/acs.jpclett.9b01619
J. Phys. Chem. Lett. 2019, 10, 3914−3921

We also drew the energy bands of Cd_3As_2/organic thin film heterojunction photodetectors (Figure 3d) to better explain the working mechanism. The prepared Cd_3As_2 thin film is tested as an N type by the Hall effect test system (Figure S7). The P−N junction is formed between Cd_3As_2 and organics, and the direction of E_{in} points from Cd_3As_2 toward the organics. When the device is being irradiated, photogenerated electrons/holes are generated at the interface between Cd_3As_2 and organics, and then they separate in the junction region because of a built-in electric field. Finally, the corresponding photocurrent is generated by the collection of electrodes.

In addition, the time-resolved femtosecond pump detection technology is used to extract the relaxation time of Cd_3As_2/organic thin films. As shown in Figure 4a, the light with a relatively stronger intensity is called the pump, which is used to excite the sample. The weaker light is called the probe, which is used to detect the nonlinear absorption effect of the sample.[45−47] As shown in Figure 4b, the detector simultaneously collects the pump and probe at the same places in the sample. At the beginning of the measurement, the probe arrives at the sample before the pump. When the probe reaches the sample behind the pump, the sample has been excited, and then the probe can measure the transmittance (reflectivity) under different delays, which corresponds to the relaxation state of the sample. By analyzing the transmittance (reflectivity) under different delay times (after excitation), we can obtain the relaxation time of the sample (Figure 4c). The methods described above were used to test the relaxation time of different thin films, and the values are 4.30 ps (Cd_3As_2), 5.87 ps (Cd_3As_2/Pedot:PSS), and 6.43 ps (Cd_3As_2/DPEPO).

Table S1 compares the properties of different Cd_3As_2-based devices in this experiment and similar devices in the previous report. Then, after more closely studying the Cd_3As_2 and other 3D Weyl material-based devices in recent years, we find that all aspects of Cd_3As_2/PEDOT:PSS and Cd_3As_2/DPEPO thin film heterojunction photodetectors are conspicuously enhanced (R_i, wavelength range, τ_{on}/τ_{off}, and on−off ratio). All the findings mentioned above can fully demonstrate that the combination of Cd_3As_2 with organics has a bright future in the preparation of MIR to LIR devices.[48−50]

In summary, we successfully prepared 3D Dirac Cd_3As_2/organic (small molecules and polymers) thin film heterojunction photodetectors in this work. It is remarkable that these inorganic/organic thin film heterojunction photodetectors exhibit a broadband response wavelength from the UV (365 nm) to the LIR (10600 nm) with fast τ_{on} (282 μs) and τ_{off} (517 μs) times at room temperature. Also, what is unexpected is the fact that the maximum of R_i of Cd_3As_2/organic heterojunction photodetectors can reach 729 mA/W; meanwhile, the corresponding EQE can reach 112%, which is significantly improved versus that of quantum Cd_3As_2-based devices. Simultaneously, the inorganic/organic heterojunction photodetectors have on−off ratios of ≤6268, which is a breakthrough in the application of 3D Dirac materials. Additionally, the femtosecond pump detection method is ingeniously used to measure the relaxation time of Cd_3As_2/organic thin film materials to study the effects of different organic materials on the fast dynamic mechanism of Cd_3As_2. Considering the fact that these Cd_3As_2/organic thin film heterojunction photodetectors possess excellent broadband responsiveness compared with that of the former Cd_3As_2-based detection systems, our work provides a completely new method for applying 3D Dirac and organic materials in photoelectric devices.

EXPERIMENTAL SECTION

Sample Preparation. Cd_3As_2 thin films are produced with a PerkinElmer (Waltham, MA) 425B MBE system. Cd_3As_2 (99.9999%) is loaded into a Knudsen cell to be vaporized onto mica substrates, and then the temperature of mica substrate remains at 170 °C with Cd and As shutters opened at the same time during the growth process.[51−54] In this experiment, a DPEPO thin film is fabricated by using organic thermal evaporation equipment to plate the evaporating material on the Cd_3As_2 thin films with a metal mask placed in advance. During this process, the vacuum is 4×10^{-4} Pa and the thin film growth rate is 0.05 nm/s. In addition, to make a good interface between the two thin films, the material evaporation temperature remains 145 °C. After the laminated thin film is prepared, the electrode is made by the method of electron beam evaporation, with an evaporation rate of 0.1 nm/s and a thickness of 80 nm. The channel length and width of the two prepared devices are 500 and 100 μm, respectively. On the other hand, the combination of polymers (PEDOT:PSS) with Cd_3As_2 thin films is fabricated by the method of spraying. The mixed ink is first loaded into the barrel of the spray pen, and then the mixed ink is sprayed onto the Cd_3As_2 thin films (5 mm × 5 mm) with a metal mask. During this experiment, the *in situ* annealing method is performed at 80 °C for 10 min. Furthermore, the nozzle diameter of the spray pen is 0.2 mm, and the N_2 pressure is 0.1 mPa. To make the thin films even and flat, a low-rate (0.05 mL/min), low-concentration (1 wt %) spraying method is used. Moreover, to make most of the solvent evaporate from the sprayed droplets during the process of falling into the substrate, which is convenient for the accumulation of the polymers on the surface of the substrate, we must guarantee that difference in height between the substrate and the spray gun is 18 cm.

Characterization of Materials. In this experiment, AFM (Asylum Research MFP-3D) was used to characterize the surface undulation of Cd_3As_2, DPEPO, and PEDOT:PSS thin films.

Characterization of Devices. In this experiment, a digital source meter (Keithley 2636B) is used to measure the photocurrent conversion performance of devices. The device response time measurement is performed by a built test platform that includes a digital source meter, a current amplifier (SR570), a pulse signal source (Rigol DG1022U), and an oscilloscope (InfiniiVision DXO-X 2024A). For pump−probe measurements, one type of 1 kHz, 800 nm, femtosecond amplifier serves as an optical source to pump a light conversion (OPA) to produce 100 fs mid-IR radiation with a range of wavelength from 2.5 to 15 μm. The probe intensity is detected by an infrared systems development corporation photodetector (INSB) and a lock-in amplifier (SR830) as a 500 Hz mechanical chopper. There tests are conducted under standard atmospheric pressure at room temperature.

ASSOCIATED CONTENT

Supporting Information

The Supporting Information is available free of charge on the ACS Publications website at DOI: 10.1021/acs.jpclett.9b01619.

DOI: 10.1021/acs.jpclett.9b01619
J. Phys. Chem. Lett. 2019, 10, 3914−3921

Production process diagram of Cd_3As_2/organic thin film heterojunction devices and AFM surface topography of the surface of Cd_3As_2 thin films (PDF)

AUTHOR INFORMATION

Corresponding Authors

*E-mail: wjun@uestc.edu.cn.
*E-mail: faxian@fudan.edu.cn.

ORCID

Jun Wang: 0000-0003-2370-2964
Guorong Wu: 0000-0002-0212-183X
Zhiming Wu: 0000-0003-3217-1376
Faxian Xiu: 0000-0003-2860-0369

Author Contributions

J.W. and F.X. guided and conceived the work. Q.Z. and M.Y. performed the data measurements and analysis. J.G., Z.W., and C.J. provided suggestions for the revision of the manuscript. All authors participated in the examination and discussion of the manuscript.

Notes

The authors declare no competing financial interest.

ACKNOWLEDGMENTS

This work is partially supported by the Science Fund for Creative Research Groups of the National Natural Science Foundation of China (61421002) and the National Natural Science Foundation of China (61674040 and 61875031).

REFERENCES

(1) Gan, X.; Shiue, R. J.; Gao, Y.; Meric, I.; Heinz, T. F.; Shepard, K.; Hone, J.; Assefa, S.; Englund, D. Chip-Integrated Ultrafast Graphene Photodetector with High Responsivity. *Nat. Photonics* **2013**, *7*, 883−887.

(2) Li, J.; Niu, L.; Zheng, Z.; Yan, F. Photosensitive Graphene Transistors. *Adv. Mater.* **2014**, *26*, 5239−5273.

(3) Huo, N.; Konstantatos, G. Recent Progress and Future Prospects of 2D-Based Photodetectors. *Adv. Mater.* **2018**, *30*, No. 1801164.

(4) Abraham, J.; Vasu, K. S.; Williams, C. D.; Gopinadhan, K.; Su, Y.; Cherian, C. T.; Dix, J.; Prestat, E.; Haigh, S. J.; Grigorieva, I. V.; Carbone, P.; Geim, A. K.; Nair, R. R. Tunable Sieving of Ions Using Graphene Oxide Membranes. *Nat. Nanotechnol.* **2017**, *12*, 546−550.

(5) Han, J.; Wang, J.; Yang, M.; Kong, X.; Chen, X.; Huang, Z.; Guo, H.; Gou, J.; Tao, S.; Liu, Z.; Wu, Z.; Jiang, Y.; Wang, X. Graphene/Organic Semiconductor Heterojunction Phototransistors with Broadband and Bi-directional Photoresponse. *Adv. Mater.* **2018**, *30*, 1804020.

(6) Oh, S.; Park, S. K.; Kim, J. H.; Cho, I.; Kim, H. J.; Park, S. Y. Patterned Taping: A High-Efficiency Soft Lithographic Method for Universal Thin Film Patterning. *ACS Nano* **2016**, *10*, 3478−3485.

(7) Zhang, E.; Wang, P.; Li, Z.; Wang, H.; Song, C.; Huang, C.; Chen, Z. G.; Yang, L.; Zhang, K.; Lu, S.; Wang, W.; Liu, S.; Fang, H.; Zhou, X.; Yan, H.; Zou, J.; Wan, X.; Zhou, P.; Hu, W.; Xiu, F. Tunable Ambipolar Polarization-Sensitive Photodetectors Based on High-Anisotropy $ReSe_2$ Nanosheets. *ACS Nano* **2016**, *10*, 8067−8077.

(8) Koppens, F. H.; Mueller, T.; Avouris, P.; Ferrari, A. C.; Vitiello, M. S.; Polini, M. Photodetectors Based on Graphene, Other Two-Dimensional Materials and Hybrid Systems. *Nat. Nanotechnol.* **2014**, *9*, 780−793.

(9) Wang, J.; Han, J.; Chen, X.; Wang, X. Design Strategies for Two Dimensional Material Photodetectors to Enhance Device Performance. *InfoMat* **2019**, *1*, 33−53.

(10) Moll, P. J.; Nair, N. L.; Helm, T.; Potter, A. C.; Kimchi, I.; Vishwanath, A.; Analytis, J. G. Transport Evidence for Fermi-Arc-Mediated Chirality Transfer in the Dirac Semimetal Cd_3As_2. *Nature* **2016**, *535*, 266−270.

(11) Wang, H.; Wang, H.; Liu, H.; Lu, H.; Yang, W.; Jia, S.; Liu, X. J.; Xie, X. C.; Wei, J.; Wang, J. Observation of Superconductivity Induced by a Point Contact on 3D Dirac Semimetal Cd_3As_2 Crystals. *Nat. Mater.* **2016**, *15*, 38−42.

(12) Yang, Y.; Gao, Z.; Xue, H.; Zhang, L.; He, M.; Yang, Z.; Singh, R.; Chong, Y.; Zhang, B.; Chen, H. Realization of a Three-Dimensional Photonic Topological Insulator. *Nature* **2019**, *565*, 622−626.

(13) Schumann, T.; Galletti, L.; Kealhofer, D. A.; Kim, H.; Goyal, M.; Stemmer, S. Observation of the Quantum Hall Effect in Confined Films of the Three-Dimensional Dirac Semimetal Cd_3As_2. *Phys. Rev. Lett.* **2018**, *120*, 016801.

(14) Mehew, J. D.; Unal, S.; Torres Alonso, E.; Jones, G. F.; Fadhil Ramadhan, S.; Craciun, M. F.; Russo, S. Fast and Highly Sensitive Ionic-Polymer-Gated WS_2-Graphene Photodetectors. *Adv. Mater.* **2017**, *29*, 1700222.

(15) Im, J. H.; Jang, I. H.; Pellet, N.; Gratzel, M.; Park, N. G. Growth of $CH_3NH_3PbI_3$ Cuboids with Controlled Size for High-Efficiency Perovskite Solar Cells. *Nat. Nanotechnol.* **2014**, *9*, 927−932.

(16) Liang, T.; Gibson, Q.; Ali, M. N.; Liu, M.; Cava, R. J.; Ong, N. P. Ultrahigh Mobility and Giant Magnetoresistance in the Dirac Semimetal Cd_3As_2. *Nat. Mater.* **2015**, *14*, 280−284.

(17) Jia, Z.; Li, C.; Li, X.; Shi, J.; Liao, Z.; Yu, D.; Wu, X. Thermoelectric Signature of the Chiral Anomaly in Cd_3As_2. *Nat. Commun.* **2016**, *7*, 13013.

(18) Jenkins, G. S.; Lane, C.; Barbiellini, B.; Sushkov, A. B.; Carey, R. L.; Liu, F.; Krizan, J. W.; Kushwaha, S. K.; Gibson, Q.; Chang, T.-R.; Jeng, H.-T.; Lin, H.; Cava, R. J.; Bansil, A.; Drew, H. D. Three-Dimensional Dirac Cone Carrier Dynamics in Na_3Bi and Cd_3As_2. *Phys. Rev. B: Condens. Matter Mater. Phys.* **2016**, *94*, 085121.

(19) Yuan, X.; Tang, L.; Liu, S.; Wang, P.; Chen, Z.; Zhang, C.; Liu, Y.; Wang, W.; Zou, Y.; Liu, C.; Guo, N.; Zou, J.; Zhou, P.; Hu, W.; Xiu, F. Arrayed Van Der Waals Vertical Heterostructures Based on 2D GaSe Grown by Molecular Beam Epitaxy. *Nano Lett.* **2015**, *15*, 3571−3577.

(20) Zhang, C.; Zhang, Y.; Yuan, X.; Lu, S.; Zhang, J.; Narayan, A.; Liu, Y.; Zhang, H.; Ni, Z.; Liu, R.; Choi, E. S.; Suslov, A.; Sanvito, S.; Pi, L.; Lu, H. Z.; Potter, A. C.; Xiu, F. Quantum Hall Effect Based on Weyl Orbits in Cd_3As_2. *Nature* **2019**, *565*, 331−336.

(21) Wang, Q.; Li, C. Z.; Ge, S.; Li, J. G.; Lu, W.; Lai, J.; Liu, X.; Ma, J.; Yu, D. P.; Liao, Z. M.; Sun, D. Ultrafast Broadband Photodetectors Based on Three-Dimensional Dirac Semimetal Cd_3As_2. *Nano Lett.* **2017**, *17*, 834−841.

(22) Yavarishad, N.; Hosseini, T.; Kheirandish, E.; Weber, C. P.; Kouklin, N. Room-Temperature Self-Powered Energy Photodetector Based on Optically Induced Seebeck Effect in Cd_3As_2. *Appl. Phys. Express* **2017**, *10*, 052201.

(23) Zhu, C.; Wang, F.; Meng, Y.; Yuan, X.; Xiu, F.; Luo, H.; et al. A Robust and Tuneable Mid-Infrared Optical Switch Enabled by Bulk Dirac Fermions. *Nat. Commun.* **2017**, *8*, 14111.

(24) Yang, M.; Wang, J.; Han, J.; Ling, J.; Ji, C.; Kong, X.; Liu, X.; Huang, Z.; Gou, J.; Liu, Z.; Xiu, F.; Jiang, Y. Enhanced Performance of Wideband Room Temperature Photodetector Based on Cd_3As_2 Thin Film/Pentacene Heterojunction. *ACS Photonics* **2018**, *5*, 3438−3445.

(25) Yang, M.; Wang, J.; Zhao, Y.; He, L.; Ji, C.; Liu, X.; Zhou, H.; Wu, Z.; Wang, X.; Jiang, Y. Three-Dimensional Topological Insulator Bi_2Te_3/Organic Thin Film Heterojunction Photodetector with Fast and Wideband Response from 450 to 3500 Nanometer. *ACS Nano* **2019**, *13*, 755−763.

(26) Chen, X.; Liu, X.; Wu, B.; Nan, H.; Guo, H.; Ni, Z.; Wang, F.; Wang, X.; Shi, Y.; Wang, X. Improving the Performance of Graphene Phototransistors Using a Heterostructure as the Light-Absorbing Layer. *Nano Lett.* **2017**, *17*, 6391−6396.

(27) Pan, R.; Li, H.; Wang, J.; Jin, X.; Li, Q.; Wu, Z.; Gou, J.; Jiang, Y.; Song, Y. High-Responsivity Photodetectors Based on Formami-

DOI: 10.1021/acs.jpclett.9b01619
J. Phys. Chem. Lett. 2019, 10, 3914−3921

dinium Lead Halide Perovskite Quantum Dot-Graphene Hybrid. *Hybrid. Part. Part. Syst. Charact.* **2018**, *35*, 1700304.
(28) Fu, W. B.; Ma, H.; Wei, Y.; Jiang, K.; Fei, G. T.; De Zhang, L. Preparation and Infrared Response Properties of Vanadium Dioxide Nanowire/Carbon Nanotube Composite Film. *J. Mater. Sci.* **2017**, *52*, 7224−7231.
(29) Konstantatos, G.; Sargent, E. Nanostructured Materials for Photon Detection. *Nat. Nanotechnol.* **2010**, *5*, 391−400.
(30) Hu, P.; Wang, L.; Yoon, M.; Zhang, J.; Feng, W.; Wang, X.; Wen, Z.; Idrobo, J. C.; Miyamoto, Y.; Geohegan, D. B.; Xiao, K. Highly Responsive Ultrathin GaS Nanosheet Photodetectors on Rigid and Flexible Substrates. *Nano Lett.* **2013**, *13*, 1649−1654.
(31) Jadhav, P. J.; Mohanty, A.; Sussman, J.; Lee, J.; Baldo, M. A. Singlet Exciton Fission in Nanostructured Organic Solar Cells. *Nano Lett.* **2011**, *11*, 1495−1498.
(32) Ehrler, B.; Walker, B. J.; Bohm, M. L.; Wilson, M. W.; Vaynzof, Y.; Friend, R. H.; Greenham, N. C. In Situ Measurement of Exciton Energy in Hybrid Singlet-Fission Solar Cells. *Nat. Commun.* **2012**, *3*, 1019.
(33) Tan, C. L.; Mohseni, H. Emerging Technologies for High Performance Infrared Detectors. *Nanophotonics* **2018**, *7*, 169−197.
(34) Zhong, H.; Xu, K.; Liu, Z.; Xu, G.; Shi, L.; Fan, Y.; Wang, J.; Ren, G.; Yang, H. Charge Transport Mechanisms of Graphene/Semiconductor Schottky Barriers: A Theoretical and Experimental Study. *J. Appl. Phys.* **2014**, *115*, 013701.
(35) Feng, Y.; Ling, L.; Nie, J.; Han, K.; Chen, X.; Bian, Z.; Li, H.; Wang, Z. L. Self-Powered Electrostatic Filter with Enhanced Photocatalytic Degradation of Formaldehyde Based on Built-in Triboelectric Nanogenerators. *ACS Nano* **2017**, *11*, 12411−12418.
(36) Zhang, K.; Zhang, T.; Cheng, G.; Li, T.; Wang, S.; Wei, W.; Zhou, X.; Yu, W.; Sun, Y.; Wang, P.; Zhang, D.; Zeng, C.; Wang, X.; Hu, W.; Fan, H. J.; Shen, G.; Chen, X.; Duan, X.; Chang, K.; Dai, N. Interlayer Transition and Infrared Photodetection in Atomically Thin Type-II $MoTe_2/MoS_2$ Van Der Waals Heterostructures. *ACS Nano* **2016**, *10*, 3852−3858.
(37) Miao, J.; Song, B.; Li, Q.; Cai, L.; Zhang, S.; Hu, W.; Dong, L.; Wang, C. Photothermal Effect Induced Negative Photoconductivity and High Responsivity in Flexible Black Phosphorus Transistors. *ACS Nano* **2017**, *11*, 6048−6056.
(38) Cui, L.; Miao, R.; Wang, K.; Thompson, D.; Zotti, L. A.; Cuevas, J. C.; Meyhofer, E.; Reddy, P. Peltier Cooling in Molecular Junctions. *Nat. Nanotechnol.* **2018**, *13*, 122−127.
(39) Zhao, M.; Zhang, J.; Gao, N.; Song, P.; Bosman, M.; Peng, B.; Sun, B.; Qiu, C.-W.; Xu, Q.-H.; Bao, Q.; Loh, K. P. Actively Tunable Visible Surface Plasmons in Bi_2Te_3 and Their Energy-Harvesting Applications. *Adv. Mater.* **2016**, *28*, 3138−3144.
(40) John, R. A.; Yantara, N.; Ng, Y. F.; Narasimman, G.; Mosconi, E.; Meggiolaro, D.; Kulkarni, M. R.; Gopalakrishnan, P. K.; Nguyen, C. A.; De Angelis, F.; Mhaisalkar, S. G.; Basu, A.; Mathews, N. Ionotronic Halide Perovskite Drift-Diffusive Synapses for Low-Power Neuromorphic Computation. *Adv. Mater.* **2018**, *30*, No. 1805454.
(41) Miao, J.; Xu, Z.; Li, Q.; Bowman, A.; Zhang, S.; Hu, W.; Zhou, Z.; Wang, C. Vertically Stacked and Self-Encapsulated Van Der Waals Heterojunction Diodes Using Two-Dimensional Layered Semiconductors. *ACS Nano* **2017**, *11*, 10472−10479.
(42) Britnell, L.; Ribeiro, R. M.; Eckmann, A.; Jalil, R.; Belle, B. D.; Mishchenko, A.; Kim, Y. J.; Gorbachev, R. V.; Georgiou, T.; Morozov, S. V.; Grigorenko, A. N.; Geim, A. K.; Casiraghi, C.; Castro Neto, A. H.; Novoselov, K. S. Strong Light-Matter Interactions in Heterostructures of Atomically Thin Films. *Science* **2013**, *340*, 1311−1314.
(43) Kufer, D.; Konstantatos, G. Photo-FETs: Phototransistors Enabled by 2D and 0D Nanomaterials. *ACS Photonics* **2016**, *3*, 2197−2210.
(44) Borisenko, S.; Gibson, Q.; Evtushinsky, D.; Zabolotnyy, V.; Buchner, B.; Cava, R. J. Experimental Realization of a Three-Dimensional Dirac Semimetal. *Phys. Rev. Lett.* **2014**, *113*, 027603.
(45) Cao, Q.; Han, S. J.; Tulevski, G. S.; Zhu, Y.; Lu, D. D.; Haensch, W. Arrays of Single-Walled Carbon Nanotubes with Full Surface Coverage for High-Performance Electronics. *Nat. Nanotechnol.* **2013**, *8*, 180−186.
(46) Lin, L.; Wang, M.; Peng, X.; Lissek, E. N.; Mao, Z.; Scarabelli, L.; Adkins, E.; Coskun, S.; Unalan, H. E.; Korgel, B. A.; Liz-Marzan, L. M.; Florin, E. L.; Zheng, Y. Opto-Thermoelectric Nanotweezers. *Nat. Photonics* **2018**, *12*, 195−201.
(47) Goulielmakis, E.; Loh, Z. H.; Wirth, A.; Santra, R.; Rohringer, N.; Yakovlev, V. S.; Zherebtsov, S.; Pfeifer, T.; Azzeer, A. M.; Kling, M. F.; Leone, S. R.; Krausz, F. Real-Time Observation of Valence Electron Motion. *Nature* **2010**, *466*, 739−743.
(48) Hu, X.; Zhang, X.; Liang, L.; Bao, J.; Li, S.; Yang, W.; Xie, Y. High-Performance Flexible Broadband Photodetector Based on Organolead Halide Perovskite. *Adv. Funct. Mater.* **2014**, *24*, 7373−7380.
(49) Adinolfi, V.; Sargent, E. H. Photovoltage Field-Effect Transistors. *Nature* **2017**, *542*, 324−327.
(50) Manga, K. K.; Wang, J.; Lin, M.; Zhang, J.; Nesladek, M.; Nalla, V.; Ji, W.; Loh, K. P. High-Performance Broadband Photodetector Using Solution-Processible PbSe-TiO_2-Graphene Hybrids. *Adv. Mater.* **2012**, *24*, 1697−1702.
(51) Zhang, C.; Zhang, E.; Wang, W.; Liu, Y.; Chen, Z. G.; Lu, S.; Liang, S.; Cao, J.; Yuan, X.; Tang, L.; Li, Q.; Zhou, C.; Gu, T.; Wu, Y.; Zou, J.; Xiu, F. Room-Temperature Chiral charge Pumping in Dirac Semimetals. *Nat. Commun.* **2017**, *8*, 13741.
(52) Yuan, X.; Cheng, P.; Zhang, L.; Zhang, C.; Wang, J.; Liu, Y.; Sun, Q.; Zhou, P.; Zhang, D. W.; Hu, Z.; Wan, X.; Yan, H.; Li, Z.; Xiu, F. Direct Observation of Landau Level Resonance and Mass Generation in Dirac Semimetal Cd_3As_2 Thin Films. *Nano Lett.* **2017**, *17*, 2211−2219.
(53) Liu, Y.; Zhang, C.; Yuan, X.; Lei, T.; Wang, C.; Di Sante, D.; Narayan, A.; He, L.; Picozzi, S.; Sanvito, S.; Che, R.; Xiu, F. Gate-Tunable Quantum Oscillations in Ambipolar Cd_3As_2 Thin Films. *NPG Asia Mater.* **2015**, *7*, e221−e221.
(54) Wang, P.; Liu, S.; Luo, W.; Fang, H.; Gong, F.; Guo, N.; Chen, Z. G.; Zou, J.; Huang, Y.; Zhou, X.; Wang, J.; Chen, X.; Lu, W.; Xiu, F.; Hu, W. Arrayed Van Der Waals Broadband Detectors for Dual-Band Detection. *Adv. Mater.* **2017**, *29*, 1604439.

DOI: 10.1021/acs.jpclett.9b01619
J. Phys. Chem. Lett. 2019, 10, 3914−3921